Amorphous metal boride as a novel platform for acetylcholinesterase biosensor development and detection of organophosphate pesticides

To cite this article before publication: Xiong Lu *et al* 2018 *Nanotechnology* in press https://doi.org/10.1088/1361-6528/aaee3f

Amorphous metal boride as a novel platform for acetylcholinesterase biosensor development and detection of organophosphate pesticides

Xiong Lu, Yanshan Li, Lu Tao, Dandan Song, Yuanzhe Wang, Yan Li, Faming Gao*

Key Laboratory of Applied Chemistry, Department of Applied Chemistry, Yanshan University, Qinhuangdao 066004, P. R. China.

*** Corresponding Author E-mail: fmgao@ysu.edu.cn. Phone: 86 335 8387552. Fax: 86 335 8061569**

ABSTRACT

The exploration of new materials for modifying electrode is important to advance electrochemical biosensors. Herein, we demonstrated that amorphous bimetallic boride material (Co-2Ni-B) prepared by a simple and facile aqueous reaction is an efficient matrix to immobilize acetylcholinesterase (AChE) to construct a biosensor for the determination of organophosphate pesticides (OPs). The effects of different composition and crystallinity on its electrochemical performance are investigated. And the optimization studies of the biological transducer were also discussed. Under optimal conditions, the fabricated sensor showed good analytical performance for the determination of chlorpyrifos with a low limit of detection (2.83 pM) and a wide linear range (3 pM-300 nM). The proposed biosensor also demonstrated high reproducibility, stability and accuracy. The impressive performance was due to the excellent conductivity and the unique amorphous bimetal–metalloid complex nanostructure. These results introduces a new class of promising materials as a robust platform for biosensor applications.

1. Introduction

Environmental monitoring has attracted great attention because of the expanding exposure of chemicals in our daily life. Pesticides, especially organophosphorus pesticides (OPs) are highly toxic agricultural compounds. And they have been extensively developed and utilized to protect crops from insects and improve the agricultural productivity. But they have caused serious public concerns about food safety and human health because of their bioaccumulation effect[1]. The high toxicity of OPs to humans and animals results from their fast and irreversible binding to the acetylcholinesterase which is a serine hydrolase and plays an important role in the central nervous system. This binding will inhibit the enzyme activity and lead to the accumulation of acetylcholine in a synaptic cleft thus resulting in severe health problems and even death[2]. Moreover, the OPs can also be well absorbed from various routes[3]. Hence, the establishment of a method for rapid, sensitive, reliable, and specific determination as well as quantification of OPs in various samples is of great significance.

Until now, extensive attention have been paid to explore effective strategies for OPs detection, such as chromatography[4, 5], immunoassay[6], colorimetric assay[7], Surface-Enhanced Raman Scattering (SERS)-based strategies[8, 9] and biosensing technology[10, 11]. Among them, AChE based electrochemical biosensors represent ideally suited tools for the analysis of OPs due to the advantages of high reliability, rapid response, simple instruments, low cost, high sensitivity and on-site analysis. In

this sensing system, the acetylthiocholine chloride (ATCl) in the solution can react with the AChE which is immobilized on the surface of a working electrode to form the thiocholine (TCl). And the TCl is an electro-active substance that can generate an irreversible oxidation current. However, the exposure of AChE to OPs will result in the decline of produced TCl and the oxidation peak decreased accordingly[12-14]. The concentration of OPs is inversely proportional to the oxidation peak of TCl. Thus, the irreversible oxidation peak could act as a marker for OPs on-line monitoring.

For the fabrication of more sensitive and efficient AChE biosensors to detect pesticides, one of the most important issues is to search for advanced materials for electrode interface construction and AChE loading. With the development in nanotechnology, various nanomaterials with special properties have been provided for the fabrication of enzyme biosensors[15]. They can enhance electron transfer, make easier immobilization of enzyme, and catalyze the enzymatic reaction. Among various of nanostructured materials, metal-based nanomaterials mainly noble metal nanomaterials are commonly used[16-19]. Although the electrochemical biosensors based on noble metal nanomaterials own good performance such as good selectivity and high sensitivity via signal amplification, their scarce resources and prohibitive costs severely restrict their further large-scale applications. Meanwhile, because of the easy preparation and low cost, metal oxides are widely used. Metal oxide nanoparticles have good biocompatibility for the enzyme loading and excellent conductivity to promote the electron transfer, thereby increasing the sensitivity of the sensors[20]. However, the application of binary metal oxides and nanocomposites has

gradually dominated due to the short of effective strategies to improve the action of a separate metal oxide[11, 21]. More recently, apart from the extensive research concentrated on the nanocomposites and metal oxides, some novel kind of transition metal compounds like chalcogenides[22, 23] (S, Se) and carbides[24, 25] (or nitrides) have also turned out to be promising candidates for enzyme immobilization. These developments inspire new directions in modifier of electrodes and prompt us to test other metal-metalloid compounds for the fabrication of enzyme biosensors. Lately, with its unique short-range ordered and long-ranged disordered atomic alignment, amorphous metal borides have raised more and more concerns because of their fascinating physical and chemical properties which are originated from their high concentration of coordinatively unsaturated sites and tunable compositions[26, 27]. Moreover, coupled with their inherent high electrical conductivity, strong chemical and thermal inertness, environmentally friendly nature, low cost and easy preparation, amorphous metal borides have been widely used in energy conversion[28-30], fuel cells[27], supercapacitors[31] and so forth. In addition, the great number of under-coordinated metal atoms, and hence abundant defects, in amorphous metal borides may also provide more active sites for the immobilization of enzyme, and also promotes the electrochemical oxidation of substrate. However, the use of amorphous metal borides for enzyme immobilization to construct an electrochemical biosensor has not been reported. Thus, it is of great interest to develop an amorphous metal borides based electrochemical biosensor and further to explore the effect of amorphous structure on electrochemical biosensing performance.

Herein, the effectiveness of using amorphous metal borides as an immobilization matrix for enzyme loading to fabricate an AChE biosensor for the determination of OPs was investigated. In this work, amorphous Co-Ni-B nanomaterials were synthesized via a facile and green reduction method. The as-prepared Co-Ni-B nanomaterials were coated onto the glassy carbon electrode (GCE) surface as an immobilization matrix, and the AChE was immobilized using chitosan (CS), a well-known biocompatible polymer with good film forming ability[32, 33], for the construction of a novel biological transducer to detect chlorpyrifos. The comparison of amorphous Co-Ni-B and the corresponding crystalline counterpart as biosensors was studied. As expected, owing to the synergistic effect between the two metals and the amorphous structure, the resulting biosensor based on amorphous material exhibited excellent analytical performances such as low detection limit, high repeatability and good stability for determination of chlorpyrifos.

2. Experimental details

Nafion (NF), Acetylthiocholine chloride (ATCl), Chitosan (CS, 85% deacetylation), Acetylcholinesterase (AChE) from electric eel, type C3389, activity 500 U/mg of protein were purchased from Sigma. Chlorpyrifos was provide by LGC Promochem (Wesel, Germany). Analytical grade nickel acetate tetrahydrate, cobalt acetate tetrahydrate, sodium borohydride, sodium hydrogen phosphate and sodium dihydrogen phosphate were obtained from Aladdin. Deionized water was employed

throughout the experiment. The prepared Co-Ni-B nanostructured materials were characterized via the powder X-ray diffractometer (D/MAX-2500, Japan), X-ray photoelectron spectrometer (Kratos Axis ULTRA) and transmission electron microscopy (JEM-2010, Japan). The measurements of differential pulse voltammetry and electrochemical impedance spectroscopy were carried out with an electrochemical workstation (CHI660E, China).

The amorphous Co-Ni-B nanomaterials were prepared via a simple reduction method. In a typical synthesis program, different molar ratio of cobalt acetate tetrahydrate and nickel acetate tetrahydrate (Co/Ni = 1/1, 1/2 and 1/3) with a total amount of 3 mmol were dissolved in 60 mL of deionized water with stirring for 30 minutes at room temperature and a homogenous solution was obtained. Then the aqueous solution of sodium borohydride (10 mL, 0.9 M) was added dropwise to the mixed solution under vigorous stir. To make sure the complete reduction of all the metallic ions in the solution, excess amount of sodium borohydride was employed. The black precipitates were separated by centrifugation and thoroughly washed several times with alcohol and ultrapure water. Finally, the cleaned powder was vacuum dried at 45℃. The obtained powders synthesized with mol ratio of Co/Ni of 1/1, 1/2 and 1/3 in solution were defined as Co-1Ni-B, Co-2Ni-B and Co-3Ni-B in turn. For comparison purposes, without addition of cobalt acetate tetrahydrate or nickel acetate tetrahydrate in the initial precursor solution, Ni-B or Co-B powders were also prepared in a similar way.

Before preparation of modified electrodes, 0.3 μm and 50 nm alumina slurry

were used to polish the GCE (3 mm diameter) consecutively. Then the electrode was washed thoroughly with deionized water. And then the electrode was sonicated with alcohol and double distilled water, respectively. For the fabrication of modified electrodes, after drying the GCE with nitrogen, 5 μL of Co-Ni-B (1 mg/mL) was coated on the freshly polished electrode surface. Then the chitosan solution (0.5% W/V, 0.1 M acetic acid aqueous solution) was mixed with the AChE solution (200 U/mL, dissolved in PBS) according to a volume ratio of 10:1. And then the modified electrode was covered with 10 μL of the above mixture and dried at 4℃. The unimmobilized enzyme was removed by rinsing the electrode with pH 7.5 phosphate buffer solution. Finally, 5 μL of NF was cast onto the modified electrode. When not in use, the enzyme electrode was stored in a refrigerator at 4℃. Other modified electrodes were assembled in a similar way according to the aforementioned methods.

The prepared enzyme electrode was applied to detect chlorpyrifos. For inhibition tests, the original current response of the enzyme electrode to ATCl was first recorded through differential pulse voltammetry (DPV). And the enzyme electrode was then exposed to a standard pesticide solution containing a certain concentration for 15 minutes after the enzyme electrode was washed with PBS. In the end, the DPV measurement of the enzyme electrode were performed again in a fresh solution of ATCl. The inhibition ratio was determined using the follow formula:

$$I(\%) \equiv \frac{I_{control} - I_{exp}}{I_{control}} \times 100\%$$

where $I_{control}$ and I_{exp} represents the peak current of ATCl without and with chlorpyrifos inhibition.

3. Results and discussion

From the TEM image (Fig. 1a) and the scanning electron microscopy (SEM) image (Fig. S1), we can see that the as-synthesized Co-2Ni-B samples were composed of nanoparticles and irregular shaped sheets. The size of nanoparticles varies in the range of about 20 nm to 45 nm. Moreover, the samples also had an amorphous structure according to the selected area electron diffraction (SAED) pattern (Fig. 1a inset) which was not distinct dots, but weak halo diffraction patterns. In addition, the presence of a broad peak at $2\theta \approx 45°$ without any of sharp crystalline peaks in the XRD pattern (Fig. 1b) obviously reveals that the as-prepared products are amorphous, which is in accordance with the SAED result. The bonding interactions and the surface elemental composition of the material was analyzed via X-ray photoelectron spectroscopy (XPS). As shown in Fig. 2a, the two peaks at 792.89 eV and 777.79 eV in the Co 2p spectrum, according to some literatures[28, 29], are corresponding to the interaction of cobalt with boron in cobalt boride. And the other two peaks whose biding energy were 796.75 eV and 780.62 eV, respectively, are thought to have arisen from Co^{2+}[29]. Similarly, the two peaks in the Ni 2p spectrum (Fig. 2b) at 869.43 eV and 852.29 eV are result from the interaction of nickel with boron in nickel boride[28, 34]. The other two peaks at 873.35 eV and 855.67 eV respectively, indicate the presence of Ni^{2+}[34]. The B 1s spectrum (Fig. 2c) exhibits two peaks at 187.67 eV and 191.66 eV respectively. The former is in agreement with boron in metal borides and a

positive chemical shift of 0.67 eV is found in comparison with pure B which is because of the reverse electron transfer from boron to metal atoms, typical of amorphous metal borides[28, 29, 34]. While the latter is as a result of boron oxide species at the surface. The prevalence of surface oxides is in accordance with the core-shell structure proposed for amorphous borides, where a thin hydroxide or oxide film envelops metal borides[29], which may provide a biocompatible atmosphere for the immobilization of enzymes.

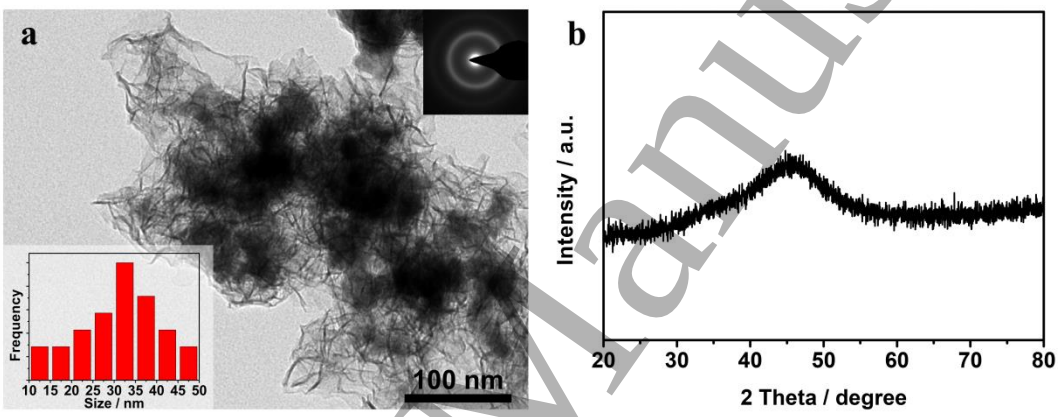

Fig. 1. TEM image (a) and XRD pattern (b) of Co-2Ni-B. Insets in panels a are the SAED pattern of Co-2Ni-B and the size distribution histogram of the nanoparticles, respectively.

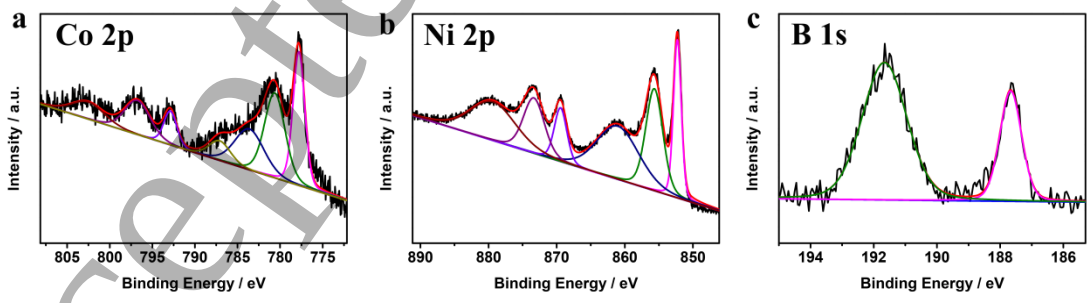

Fig. 2.(a) Co 2p, (b) Ni 2p and (c) B 1s XPS spectra of the as-prepared amorphous ternary Co-2Ni-B powders.

In this work, electrochemical impedance spectroscopy (EIS) was applied for the

evaluation of the electrochemical performance of the different electrodes. The EIS was performed in 5 mM $Fe(CN)_6^{3-/4-}$ solution containing 0.1 M KCl, and the results of the electrodes modified with different Co-Ni-B materials were shown in Fig. S2a. As what we can see, the Co-2Ni-B/GCE has the lowest electron transfer resistance. This phenomenon is probably due to the good conductivity of Co-2Ni-B, which may benefit from the synergistic effects and suitable composition of the Co-2Ni-B which makes it form a nanosheet structure and have a better dispersion as compared with the other Co-Ni-B nanomaterials (Fig. S3).

Choosing Co-2Ni-B as the electrode surface modification materials, we have also used EIS to monitor the assembly process of the enzyme electrode. In Fig. S2b, we can see that when the mixture of AChE and chitosan was cast onto Co-2Ni-B modified electrode, the electron transfer resistance increased which was because of the insulating properties of biological macromolecules and the poor conductivity of chitosan that could hinder the transmission of electrons, suggesting the fact that AChE and chitosan had been successfully immobilized on the Co-2Ni-B/GCE. And after the nafion was coated onto the CS-AChE/Co-2Ni-B/GCE, the electron transfer resistance further increased. Though the nafion could hinder the electron transfer, it could prevent the leaching of the AChE from the modified electrode[23].

Fig. S4a shows the typical differential pulse voltammetry (DPV) peaks of NF/CS-AChE/GCE and NF/CS-AChE/Co-2Ni-B/GCE in pH 7.5 PBS (0.1 M). It could be found that, no oxidation peaks were observed with the absence of ATCl in the solution. And when 5 mM ATCl was added into the solution, the response currents

appeared on both of the modified electrodes. And as expected, NF/CS-AChE/Co-2Ni-B/GCE gained a larger current peak, proving the suitability of Co-2Ni-B for enzymatic product determination. Moreover, the current responses of various electrodes which were prepared by different modified materials was measured by DPV. And the crystalline Co-2Ni-B was also tested which was obtained by annealing amorphous Co-2Ni-B at 500℃ in Ar for 2h. The SAED (Fig. S5a inset) and the XRD pattern (Fig. S5b) of the as-obtained annealed Co-2Ni-B indicate its crystalline nature. As shown in Fig. S4b, NF/CS-AChE/Co-2Ni-B/GCE has the biggest current value. The enhanced electrochemical response possibly because not only the good conductivity of Co-2Ni-B, which was in accordance with the results of EIS, but also the abundant defects in amorphous nanomaterial which may provide more active sites for enzyme immobilization and promote electrochemical oxidation of thiocholine. Therefore, based on these electrochemical analyses above, NF/CS-AChE/Co-2Ni-B/GCE was utilized for further electrochemical studies.

The biological activity of enzyme immobilized on the electrode exhibits an important dependence on the pH value. The peak current of NF/CS-AChE/Co-2Ni-B/GCE to 5 mM ATCl was explored in a series of phosphate buffer solution with pH range from 6 to 8.5. As what we can see in Fig. S6a, when the value of pH was 7.5, the current response was maximized. This may be due to the fact that the optimum pH value of the enzyme immobilized on the electrode was 7.5, and when the pH value was higher or lower than 7.5, the activity of the enzyme would be reduced, resulting in the decline of produced thiocholine and the oxidation peak

decreased accordingly. Thus, pH 7.5 was employed for the following studies.

Also we investigated the impact of enzyme volume on the current response of NF/CS-AChE/Co-2Ni-B/GCE to ATCl. From Fig. S6b, it is obvious that as the amount of AChE raised, the response increased gradually, and when the amount of enzyme was 0.2 U, the current peak reached a maximum. However, with the enzyme volume further raised, the peak current declined. The phenomenon may be due to the blocked electronic transmission by the excessive enzyme volume since the insulating properties of the enzyme. Thus, we used 0.2 U of AChE for further studies.

The current response of the NF/CS-AChE/Co-2Ni-B/GCE to ATCl was also affected by the Co-2Ni-B volume casted on the electrode. As shown in Fig. S7, during the volume of Co-2Ni-B ranged from 1 to 5 μL, the response current increased gradually and reached the maximal value at 5 μL. When the volume of Co-2Ni-B exceeded 5 μL, the peak current decreased, possibly because of increased thickness of the added nanomaterials, which may block the electron and mass transfer. Hence, the optimal volume of Co-2Ni-B was 5 μL.

Incubation time played a critical role in the enzyme-based inhibition assay for the detection of chlorpyrifos and its influence on the biosensor performance was investigated through immersing the NF/CS-AChE/Co-2Ni-B/GCE in the chlorpyrifos solution which has a constant concentration of 0.03 μM for different times. And as the Fig. S8 showed that as the incubation time extended, the inhibition degree of the enzyme increased and obtained a platform after the incubation time exceeded 15 minutes, indicating that the combination of enzymes and pesticides reached saturation.

Thereby, we chose 15 minutes as the optimal incubation time.

At the optimum experimental parameters, the typical current-time response curve of the NF/CS-AChE/Co-2Ni-B/GCE was acquired through continuously adding ATCl to a continuously stirred phosphate buffer solution with a pH value of 7.5. As Fig. 3 shown, the current response raised with the increasing of ATCl concentration. And the oxidation current of ATCl was linear with its concentration in the range of 4-372 μM. The linear equation was $I(\mu A) = 0.0022c(\mu M) + 0.0905$ (R^2 = 0.9914) (inset a). As the ATCl concentration further increased, a platform was observed, indicating a Michaelis-Menten process. The Michaelis-Menten constant (K_M) was determined by using the Lineweaver-Burk equation[35]. In this work, the K_M value was 379 μM, which was smaller than that of 700 μM for electrochemically reduced graphene oxide based AChE electrode[36] and 730 μM for porous-reduced graphene oxide based AChE electrode[37], indicating a higher affinity of the NF/CS-AChE/Co-2Ni-B/GCE to ATCl. And this phenomenon may be due to the abundant defects in amorphous metal borides which could promote the electrochemical oxidation of substrate.

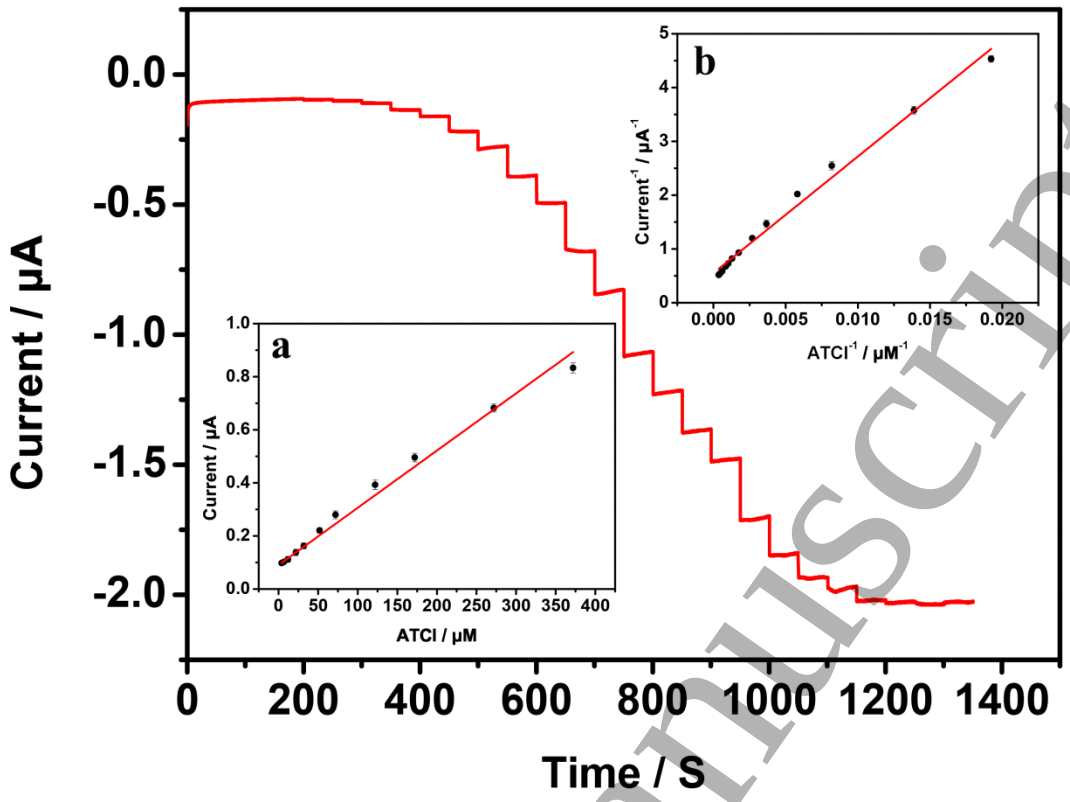

Fig. 3. The i-t plot according to the response of NF/CS-AChE/Co-2Ni-B/GCE to ATCl concentration. Applied potential: 600 mV. Insets: The linear calibration curve for ATCl detection (a) The Lineweaver-Burk curve (b).

The determination of chlorpyrifos was performed via DPV before and after the modified electrode exposure to different concentrations of chlorpyrifos in phosphate buffer solution. As Fig. 4a showed that, there was no response current at NF/CS-AChE/Co-2Ni-B/GCE (h) in the solution without ATCl. Nevertheless, the DPV exhibited a distinct current peak at 556 mV (a), when adding 5 mM of ATCl to the solution. After the enzyme electrode was exposed to different concentrations of chlorpyrifos solution, a different degree of decline in the response current has been observed. And with the increase of the chlorpyrifos concentration, the decrease in current peak increased sequentially. This is probably due to the binding interaction

between chlorpyrifos and AChE, in which the pesticide can block the active sites of AChE by covalently bound to its serine hydroxyl groups, resulting the invariably inhibition of AChE bioactivity.

Fig. 4b showed the calibration curve for inhibition rate and the concentration of chlorpyrifos. It can be found that in the chlorpyrifos concentration range from 3×10^{-12} to 3×10^{-7} M, there is an excellent linear relationship between inhibition rate and Log [chlorpyrifos]. The linear regression equation was $Inhibition(\%) = 136.95 + 10.72LogC$ (R^2=0.995). And based on the signal-to-noise at 3, the detection limit in this work was calculated to be 2.83×10^{-12} M. In addition, the analytical properties between the developed biosensor and other published biosensors which were used for chlorpyrifos detection have been compared. And from Table 1[35, 38-44], we could find that the NF/CS-AChE/Co-2Ni-B/GCE exhibited a better analytical performance, demonstrating that the Co-2Ni-B could be a fascinating candidate to construct the AChE based biosensor for pesticides detection.

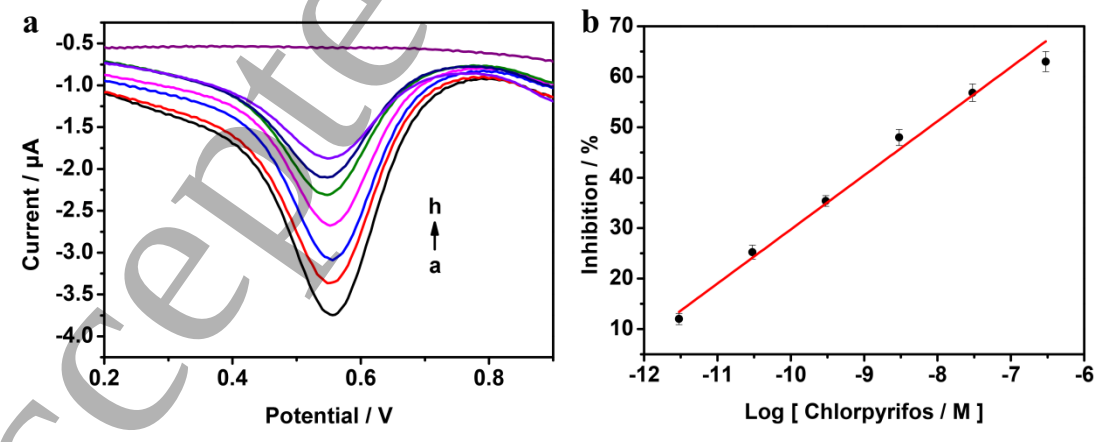

Fig. 4. (a) Differential pulse voltammetry of NF/CS-AChE/Co-2Ni-B/GCE in phosphate buffer solution without (h) or containing (a-g) 5 mM ATCl after incubation

with (a) 0, (b) 3 pM, (c) 30 pM, (d) 0.3 nM, (e) 3 nM, (f) 30 nM, (g) 0.3 μM chlorpyrifos for 15 min. (b) Inhibition curve for chlorpyrifos detection.

Table 1

Comparison with other published biosensors for chlorpyrifos determination.

Sensors	Limit of detection	Linear range	Precision (RSD)	Recovery	References
Nafion/AChE/CS-PB-MWNTs-HGNs/Au	0.05 nM	0.05 nM-75 nM	3.3%/6.7%	94%-106%	[35]
AChE/CPBA/GR-AuNPs/GCE	0.29 nM	1.4-29 nM, 29-290 nM	4.8%/6.1%	-	[38]
AChE/rGO@Pd/GCE	0.23 μM	0.7-5 μM, 5-71 μM	2.7%/3.5%	98%-112%	[39]
AChE-Fe_3O_4NPs/c-MWCNTs/ITO	0.1 nM	0.1 nM-50 nM	-	98%-99%	[40]
AChE-PVA-SbQ/PEDOT/SPE	0.01 nM	0.02 nM-10 nM	-	-	[41]
AChE/TCNQ-MWCNT/SPE	0.4 nM	1 nM-100 nM	3%/3.5%	87%-94%	[42]
BChE/MG/MnO_2/SPE	8 pM	8 pM-10 nM	-	-	[43]
AChE/[BMIM][BF_4]/MWCNT-CPE	4 nM	10 nM-1 μM	-	-	[44]
NF/CS-AChE/Co-2Ni-B/GCE	2.83 pM	3 pM-300 nM	3.8%/5.3%	96%-105%	This issue

The fabrication reproducibility of NF/CS-AChE/Co-2Ni-B/GCE was performed by using five freshly prepared enzyme electrodes to compare their response currents in the presence of ATCl. And much the same, the repeatability was carried out by 5 times repeated tests through one enzyme electrode. The RSD values were 3.8% and 5.3%, revealing a desirable precision (Fig. S9). Besides, the enzyme electrode also has a good stability. After 20 days of storage at 4℃, the enzyme electrode still remained 85% of initial activity. And during the continuous test of 10000 seconds, the

change in the response current of the biosensor was almost negligible (Fig. S10).

The interference study of the developed enzyme electrode was evaluated through comparing the signal obtained with or without the interfering agents which are commonly found in the environment such as citric acid, carbamide, glucose, Cu^{2+}, Fe^{3+}, NO_3^- and SO_4^{2-}. As Fig. S11 shown, when the aforementioned interfering agents were existed in the solution, there was no noticeable change of response currents could be detected, demonstrating acceptable selectivity of the biosensor for the determination of chlorpyrifos.

The recovery tests were used to evaluate the applicability of NF/CS-AChE/Co-2Ni-B/GCE through adding different concentration of chlorpyrifos in tap water samples. The recovery percentages ranged from 96% to 105% for the detection of chlopyrifos according to the results listed in Table S1, which suggested that the biosensor owned good accuracy and could be applied in practical samples.

4. Conclusions

In summary, an amorphous metal-boron-based material is synthesized by a simple and green approach. The as-prepared Co-2Ni-B nanomaterial was further used as a matrix to immobilize AChE to detect chlorpyrifos. Benefiting from the good conductivity and abundant defects of amorphous Co-2Ni-B which may provide more active sites for the effective electrocatalytic oxidation of TCl, the developed AChE biosensor demonstrated high reproducibility, good stability, wide linear range and low detection limit. Moreover, in the real sample analysis with tap water, high recoveries were also

achieved. The study not only demonstrates the possible application of amorphous metal boride in the field of biosensors, but also introduces a new class of promising materials for the sensing platform.

Acknowledgments

The authors acknowledge the financial support from the National Natural Science Foundation of China (Grant No. 21875205, 21671168) and the Natural Science Foundation of Hebei (Grant No. B2016203498, 17964403D) .

References

[1] Aragay G, Pino F and Merkoçi A 2012 *Chem. Rev.* 112 5317
[2] Kumar P, Kim K H and Deep A 2015 *Biosens. Bioelectron.* 70 469
[3] Colovic M B, Krstic D Z, Lazarecuc-Pasti T D, Bondzic A M and Vasic V M 2013 *Curr. Neuropharmacol.* 11 315
[4] Zhou T, Xiao X and Li G 2012 *Anal. Chem.* 84 5816
[5] Roca M, Leon N, Pastor A and Yusa V 2014 *J. Chromatogr. A* 1374 66
[6] Liu C, Jia Q, Yang C, Qiao R, Jing L, Wang L, Xu C and Gao M 2011 *Anal. Chem.* 83 6778
[7] Zhang S, Xue S, Deng J, Zhang M, Shi G and Zhou T 2016 *Biosens. Bioelectron.* 85 457
[8] Liang X, Wang Y S, You T T, Zhang X J, Yang N, Wang G S and Yin P G 2017 *Nanoscale* 9 8879
[9] Jiang T, Zhang L, Jin H, Wang X L and Zhou J 2015 *Dalton Trans.* 44 7606
[10] Caballero-Diaz E, Benitez-Martinez S and Valcarcel M 2017 *Sens. Actuators B: Chem.* 240 90
[11] Cui H, Wu W, Li M, Song X, Lv Y and Zhang T 2018 *Biosens. Bioelectron.* 99 223
[12] Schulze H, Vorlova S, Villatte F, Bachmann T and Schmid R 2003 *Biosens. Bioelectron.* 18 201
[13] Wei M and Wang J 2015 *Sens. Actuators B: Chem.* 211 290
[14] Yu G, Wu W, Zhao Q, Wei X and Lu Q 2015 *Biosens. Bioelectron.* 68 288
[15] Kurbanoglu S, Ozkan S A and Merkoci A 2017 *Biosens. Bioelectron.* 89 886
[16] Guler M, Turkoglu V and Basi Z 2017 *Electrochim. Acta* 240 129
[17] Lu X, Tao L, Song D, Li Y and Gao F 2018 *Sens. Actuators B: Chem.* 255 2575

[18] Zhao H, Ji X, Wang B, Wang N, Li X, Ni R and Ren J 2015 *Biosens. Bioelectron.* 65 23
[19] Upadhyay S, Rao G R, Sharma M K, Bhattacharya B K, Rao V K and Vijayaraghavan R 2009 *Biosens. Bioelectron.* 25 832
[20] Sundarmurugasan R, Gumpu M B, Ramachandra B L, Nesakumar N, Sethuraman S, Krishnan U M and Rayappan J B 2016 *Sens. Actuators B: Chem.* 230 306
[21] Maduraiveeran G, Sasidharan M and Ganesan V 2018 *Biosens. Bioelectron.* 103 113
[22] Nasir M, Mayorga-Martinez C, Sofer Z and Pumera M 2017 *ACS Nano* 11 5774
[23] Peng L, Dong S, Wei W, Yuan X and Huang T 2017 *Biosens. Bioelectron.* 92 563
[24] Zhou L, Zhang X, Ma L, Gao J and Jiang Y 2017 *Biochem. Eng. J.* 128 243
[25] Wu L, Lu X, Dhanjai, Wu Z, Dong Y, Wang X, Zheng S and Chen J 2018 *Biosens. Bioelectron.* 107 69
[26] Carenco S, Portehault D, Boissiere C, Mezailles N and Sanchez C 2013 *Chem. Rev.* 113 7981
[27] He D, Zhang L, He D S, Zhou G, Lin Y, Deng Z, Hong X, Wu Y, Chen C and Li Y 2016 *Nat. Commun.* 7 12362
[28] Nsanzimana J M, Peng Y, Xu Y Y, Thia L, Wang C, Xia B Y and Wang X 2018 *Adv. Energy Mater.* 8 1701475
[29] Masa J, Weide P, Peeters D, Sinev I, Xia W, Sun Z, Somsen C, Muhler M and Schuhmann W 2016 *Adv. Energy Mater.* 6 1502313
[30] Li L, Deng Z, Yu L, Lin Z, Wang W and Yang G 2016 *Nano Energy* 27 103
[31] Chen R, Liu L, Zhou J, Hou L and Gao F 2017 *J. Power Sources* 341 75
[32] Jeyapragasam T and Saraswathi R 2014 *Sens. Actuators B: Chem.* 191 681
[33] Song D, Li Y, Lu X, Sun M, Liu H, Yu G and Gao F 2017 *Anal. Chim. Acta* 982 168
[34] Masa J, Sinev I, Mistry H, Ventosa E, Mata M, Arbiol J, Muhler M, Cuenya B R and Schuhmann W 2017 *Adv. Energy Mater.* 7 1700381.
[35] Zhai C, Sun X, Zhao W, Gong Z and Wang X 2013 *Biosens. Bioelectron.* 42 124
[36] Wu S, Huang F, Lan X, Wang X, Wang J and Meng C 2013 *Sens. Actuators B: Chem.* 177 724
[37] Li Y, Bai Y, Han G and Li M 2013 *Sens. Actuators B: Chem.* 185 706
[38] Liu T, Su H, Qu X, Ju P, Cui L and Ai S 2011 Sens. Actuators B: Chem. 160 1255
[39] Zhang Y, Xia Z, Li Q, Gui G, Zhao G and Lin L 2017 *J. Electrochem. Soc.* 164 48
[40] Chauhan N and Pundir C S 2012 *Electrochim. Acta* 67 79
[41] Istamboulie G, Durbiano R, Fournier D, Marty J L and Noguer T 2010 *Chemosphere* 78 1
[42] Rotariu L, Zamfir L G and Bala C 2012 *Anal. Chim. Acta* 748 81
[43] Sigolaeva L V, Gladyr S Y, Mergel O, Gelissen A P, Noyong M, Simon U, Pergushov D V, Kurochkin I N, Plamper F A and Richtering W 2017 *Anal. Chem.* 89 6091

[44] Zamfir L G, Rotariu L and Bala C 2011 *Biosens. Bioelectron.* 26 3692